ELSEVIER

Journal of Alloys and Compounds 293–295 (1999) 231–236

Journal of ALLOYS AND COMPOUNDS

Calculation of the radial distribution function of bubbles in the aluminum hydrogen system

C.E. Buckley[a,*], H.K. Birnbaum[b], D. Bellmann[c], P. Staron[c]

[a]*Department of Applied Physics, Curtin University of Technology, GPO Box U 1987, Perth 6845, WA, Australia*
[b]*Materials Research Laboratory, University of Illinois, Urbana, IL 61801, USA*
[c]*Institute for Materials Research, GKSS-Research Centre, Geesthacht GmbH, D-21502 Geesthacht, Germany*

Abstract

Aluminum foils of 99.99% purity were charged with hydrogen using a gas plasma method with a voltage in the range of 1.0–1.2 keV and current densities ranging from 0.66 to 0.81 mA cm^{-2}, resulting in the introduction of a large amount of hydrogen. X-ray diffraction measurements indicated that within experimental error there was a zero change in lattice parameter after plasma charging. This result is contradictory to almost all other FCC materials, which exhibit a lattice expansion when the hydrogen enters the lattice interstitially. It is hypothesised that the hydrogen does not enter the lattice interstitially, but instead forms a H-vacancy complex at the surface which diffuses into the volume and then clusters to form H_2 bubbles. The nature and agglomeration of the bubbles were studied with a variety of techniques, such as small angle, ultra small angle and inelastic neutron scattering (SANS, USANS and INS), transmission and scanning electron microscopy (TEM and SEM), precision density measurements (PDM) and X-ray diffraction. The USANS and SANS results indicated scattering from a wide range of bubble sizes from <10 Å up to micron size bubbles. Subsequent SEM and TEM measurements revealed the existence of bubbles on the surface, as well as in the bulk and INS experiments show that hydrogen is in the bulk in the form of H_2 molecules. In this paper we calculate the radial distribution function of the bubbles from the SANS and USANS results using methods based on the models derived by Brill et al., Fedorova et al. and Mulato et al. The scattering is assumed to be from independent spherical bubbles. Mulato et al. model is modified by incorporating smearing effects, which consider the instrumental resolution of the 30 m SANS spectrometer at NIST. The distribution functions calculated from the two methods are compared, and these distributions are then compared with the range of particle sizes found from TEM and SEM techniques.

Keywords: SANS; USANS; Modeling; Hydrogen-vacancy complex; Aluminum

1. Introduction

Small angle neutron (SANS) [1,2] and X-ray (SAXS) [3,4] scattering are well established techniques for the investigation of nonperiodic structures with dimensions between 10 and several thousand Å. Recent advances in the reduction of the inherent background from channel cut crystals used for ultra small angle neutron scattering (USANS) experiments, enables investigation of particle sizes approaching 70 μm [5,6]. Data from USANS, SANS and SAXS experiments can be used to determine a particle size distribution in a polydisperse system. However the analysis of a particle size distribution in a polydisperse system is an ill posed problem due to the inverse relationship between the scattering intensity ($I(q)$) and the size distribution ($D(r)$) being calculated from a limited range of experimental data [7].

Mulato et al. [7] showed that their recurrence numerical corrector method was superior to the use of Tikhonov's regularization technique from Svergun et al. [8] and also superior to termination corrector methods proposed by Brill et al. [9] and Brill and Schmidt [10], when applied to ideal data (not experimental data). Mulato et al. [11] further show that their method is robust, when noise is introduced to the ideal data.

In this paper we test the termination corrector methods [9,10] (Model I) and the recurrence numerical corrector method [7] (Model II) on experimental SANS and USANS data for the aluminum–hydrogen system [12–14]. Both methods are used in conjunction with Fedorova and Schmidt's [15] analytical expression for the distribution of hard spheres, since it is assumed that the H_2 bubbles in Al are spherical in nature. Model II is modified by including smearing effects caused by the instrumental resolution of the 30 m SANS spectrometer at The National Institute of Standards and Technology (NIST), Gaithersburg.

*Corresponding author.

0925-8388/99/$ – see front matter
PII: S0925-8388(99)00425-9

It is found that the distribution function calculated from Model I returns negative values, a physically unreasonable result, in the distribution function that describes the number of hydrogen bubbles as a function of radius, whereas the distribution calculated from Model II agrees quantitatively with an approximate distribution found from SEM and TEM results [16]. The agreement between calculated and experimental intensities is good at low q (the reciprocal lattice vector) but falls away at high q values.

2. Experimental

Polycrystalline Al foils of 99.99% purity that were ≈130 μm thick, were annealed for 24 h in a vacuum of 10^{-4} Pa at 560°C. Four foils were then charged with hydrogen at room temperature for 76 h using a H_2 plasma charging technique using acceleration voltages ranging from 1 to 1.2 keV and a current density of 0.68 mA cm^{-2}. The average hydrogen concentration of the foils was determined by prompt gamma activation analysis (PGAA) [17] and gas chromatography and was found to be 2100±50 ppm. The average integrated number of protons impinging on the foils was 1.41×10^{21} cm^{-2}. Given that the concentration of H atoms in the foil was 2.1×10^{-3}, only 0.12% of the protons diffused into the bulk. The distribution of the hydrogen and the point defects created by 1 keV H^+ ions impinging on the aluminum foil were calculated using the TRIM code. The average depth of the implanted H ions and the point defects created by the H ions was found to be ≈194 Å which is 0.015% of the specimen thickness.

The SANS experiment was conducted on the foils utilising the 30 m SANS instrument at NIST, using a wavelength of 8 Å and three sample to detector distances, 1.3, 4.5 and 13.17 m. Scattering cross sections $d\Sigma/d\Omega$ or intensity (I(q)) were measured over the range $0.0019<q<0.32$ $Å^{-1}$, where $q=4\pi\sin\theta/\lambda$ (2θ is the scattering angle and λ is the wavelength).

The USANS experiment was performed by means of the double crystal diffractometer (DCD) using a wavelength of 4.43 Å at the Geesthacht Neutron Facility (GeNF). The reciprocal lattice vector ranged from $q=2.6\times10^{-5}$ to 4.0×10^{-4} $Å^{-1}$. The differential cross sections from the USANS data were de-smeared and can be compared directly to data from pinhole geometry.

3. Results and discussion

Experimental results from USANS, SANS, TEM, SEM and inelastic neutron scattering (INS) show that the hydrogen is in the aluminum as H_2 bubbles [16]. The following analysis assumes the bubbles are independent spherical particles.

The termination corrector method [9,10] (Model I) for calculating a distribution function from the experimental (q,I) data relies on extrapolating the (q,I) data from the minimum SANS experimental q value (q_{min}) to $q=0$ and from the maximum SANS q value (q_{max}) to $q=4$. From the USANS results, (q,I) is known in the q range 2.6×10^{-5} $Å^{-1}$ to q_{min}, and is extrapolated back to $q=0$, therefore there is no need to extrapolate the SANS data back to the low q region. I(q) for $q=q_{max}$ to ∞ is found using an extrapolation method developed by Brill et al. [9], where for large q, I(q) will have the form

$$\mathrm{I}(q) = C_4\, q^{-4} + C_6\, q^{-6} + C_8\, q^{-8} \tag{1}$$

Eqs. (2– 4) form a set of three algebraic equations, which define the constants C_4, C_6 and C_8

$$q_{max}^4\, \mathrm{I}(q_{max}) = C_4 + C_6\, q_{max}^{-2} + C_8\, q_{max}^{-4} \tag{2}$$

$$q_{max}^{-1} \int_0^{q_{max}} q^4 \mathrm{I}(q)\mathrm{d}q = C_4 - C_6\, q_{max}^{-2} - \frac{C_8\, q_{max}^{-4}}{3} \tag{3}$$

$$q_{max}^{-3} \int_0^{q_{max}} q^6 \mathrm{I}(q)\mathrm{d}q = \tfrac{C_4}{3} + C_6\, q_{max}^{-2} - C_8\, q_{max}^{-4} \tag{4}$$

The determination of C_4, C_6 and C_8 from the experimental and extrapolated data must satisfy the criteria that a reliable extrapolation of an experimental scattering curve for spherical particles returns a positive value for C_6 [9]. A particle distribution function, D(r) can now be calculated using the scattering data for all q from 0 to ∞, where $q=\infty$ is satisfied by Eq. (5)

$$C_4 = \lim_{q\to\infty} q^4 \mathrm{I}(q) \tag{5}$$

Assuming the particles are a distribution of non-interacting spheres it can be shown that [15] (note that there is a mistake in the original paper)

$$\mathrm{D}(r) = \frac{A}{r^2}\int_0^{\infty} (\mathrm{I}(q)\, q^4 - C_4)\left[\cos 2x\left(1-\frac{2}{x^2}\right) - \frac{2\sin 2x}{x}\left(1-\frac{1}{2x^2}\right)\right]\mathrm{d}q \tag{6}$$

where $x=qr$, and r is the radius of the sphere and A is a normalisation constant. The distribution at $r\to\infty$ is found by placing a limit on the radius of the bubble which is consistent with the experimental data. From the USANS data the intensity was extrapolated down to $q=0$, but only scattering effects from bubble sizes which are correlated to a value greater than the Darwin width are detectable. In this case the maximum particle size is $r\approx\pi/q_{min}$ ($q_{min}\approx 2.6\times10^{-5}$ $Å^{-1}$), therefore the maximum value of r was set at 12.1 μm.

The Mulato et al. [7] model (Model II) is based on a recursion method, which does not involve extrapolation of the experimental data. The fixed-point iteration can be written as [18]

$$D_{k+1} = D_k + P_2\{T_3[I - T_1(D_k)]\} \quad (7)$$

where P_2 represents the projector operator on the physical subspace to which each D(r) belongs. For details of P_2 see Ref. [7]. $T_1(D_k)$ is described by Eq. (8)

$$T_1(D_k) = \int_0^\infty D(r)\, I_o(q,r)dr \quad (8)$$

where r_{min} and r_{max} replace 0 and ∞ in (8) and $I_0(q,r)$ (see (9)) is the scattered intensity from a single particle with characteristic radius, r

$$I_0(q,r) = \frac{J_{3/2}^2(qr)}{(qr)^3} r^6 \quad (9)$$

where

$$J_{3/2}(qr) = \left(\frac{2}{\pi qr}\right)^{1/2}\left(\frac{\sin(qr)}{qr} - \cos(qr)\right) \quad (10)$$

At this point we modify Model II by introducing a resolution function [19] to the model. The resolution function $R(q_1,q)$ describes the distribution of scattering vectors with length q_1, which contribute to the scattering for the nominal scattering vector length, q, corresponding to the instrument configuration.

$$R(q_1,q) = \frac{f_s}{\sqrt{2\pi V_q}} e\left(\frac{-(q_1-\bar{q})^2}{2V_q}\right) \quad (11)$$

where $V_q = \sigma^2$ is the variance in the momentum transfer q_1, f_s is the shadow factor and $\bar{q}$ is the mean scattering vector. V_q, f_s, and $\bar{q}$ are functions of q [19]. Eq. (11) is calculated for $q_1 = 0$ to ∞, where q_1 has N values from 0 to ∞ and ∞ is chosen to be that value when $R(q_1,q) < 10^{-20}$. It was found that $q_1 \leq 0.5$ returned $R(q_1,q) > 10^{-20}$ for all q, therefore $q_1 = 0.5$ was set to be ∞. The modeled intensity function $d\Sigma/d\Omega(q_1)$ is calculated in terms of q_1

$$\frac{d\Sigma}{d\Omega}(q_1) = \int_0^\infty D(r)\, I_0(q_1,r)dr \quad (12)$$

Finally (8) is modified to incorporate the resolution function

$$I_m(q) = \int_0^\infty R(q, q_1)\frac{d\sigma}{d\Omega}(q_1)dq_1 \quad (13)$$

where $I_m(q)/T_1(D)$. T_3 is the transformation described by (6) using the integration limits q_{min} and q_{max} instead of 0 to ∞ and I is the experimental SANS data. At each step a new D(r) curve is obtained based on the previous one and a convergence parameter was chosen to be the integrated area of $D_k(r)$

$$\int_{r_{min}}^{r_{max}} D_k(r)\, dr = A \quad (14)$$

where the calculation was stopped as $A \to 1$.

Fig. 1 depicts the normalised distribution function, D(r), for Model I, in the range $r = 10$–100 Å. Although D(r) is calculated from $r = 10$ Å–12.1 μm, it is only shown in the range $r = 10$–100 Å, due to the fact that it becomes very small for $r > 100$ Å. It is clear from Fig. 1 that the distribution function, D(r) for Model I oscillates from positive to negative values in a physically unrealistic manner over the r range shown, and in fact D(r) oscillates from positive to negative values over the full range, $r = 10$ Å–12.1 μm.

In contrast Model II returns a D(r) with a large peak between $r \approx 300$ and 600 Å (see Fig. 2a), and smaller peaks between 1000–1100 Å and 1500–1600 Å. Fig. 2b and c show D(r) plotted on a log scale in the r ranges 1000–1100 Å, and 1500–1621 Å. It is difficult to establish if the peaks in Figs. 2a and b have any physical significance. However, TEM images of these samples depict bubbles ranging in size from 5 to 7000 Å, with the majority of bubbles being <1000 Å [16], which agrees quantitatively with the distribution function calculated from Model II, shown in Fig. 2a. This figure also shows that D(r) for Model II decreases as $r \to 0$, which is a pleasing aspect of the model, since models used to calculate the distribution functions generally show $|D(r)|$ having a peak as $r \to 0$.

Fig. 2d shows D(r) plotted on a log scale is a smoothly decreasing function from $r = 0.1$ to 12.1 μm. SEM images

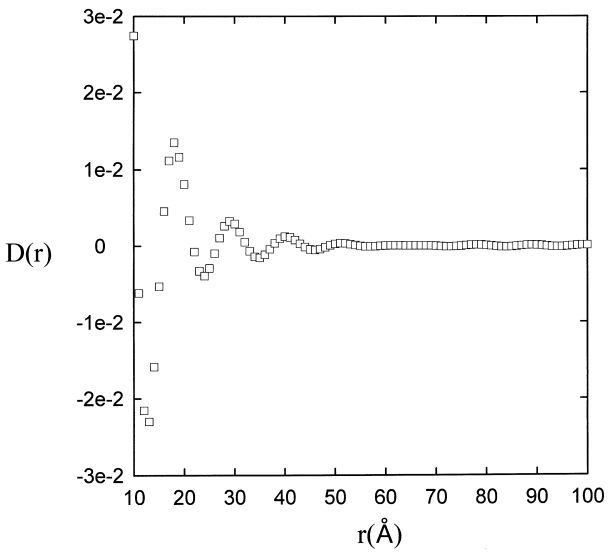

Fig. 1. Distribution function, D(r), calculated for SANS data from Mode1 I (G) in the range $r = 10$–100 Å showing the oscillatory nature of D(r). The r range, $r > 100$ Å is not shown since $D(r) \to 0$ as $r \to 12.1$ μm.

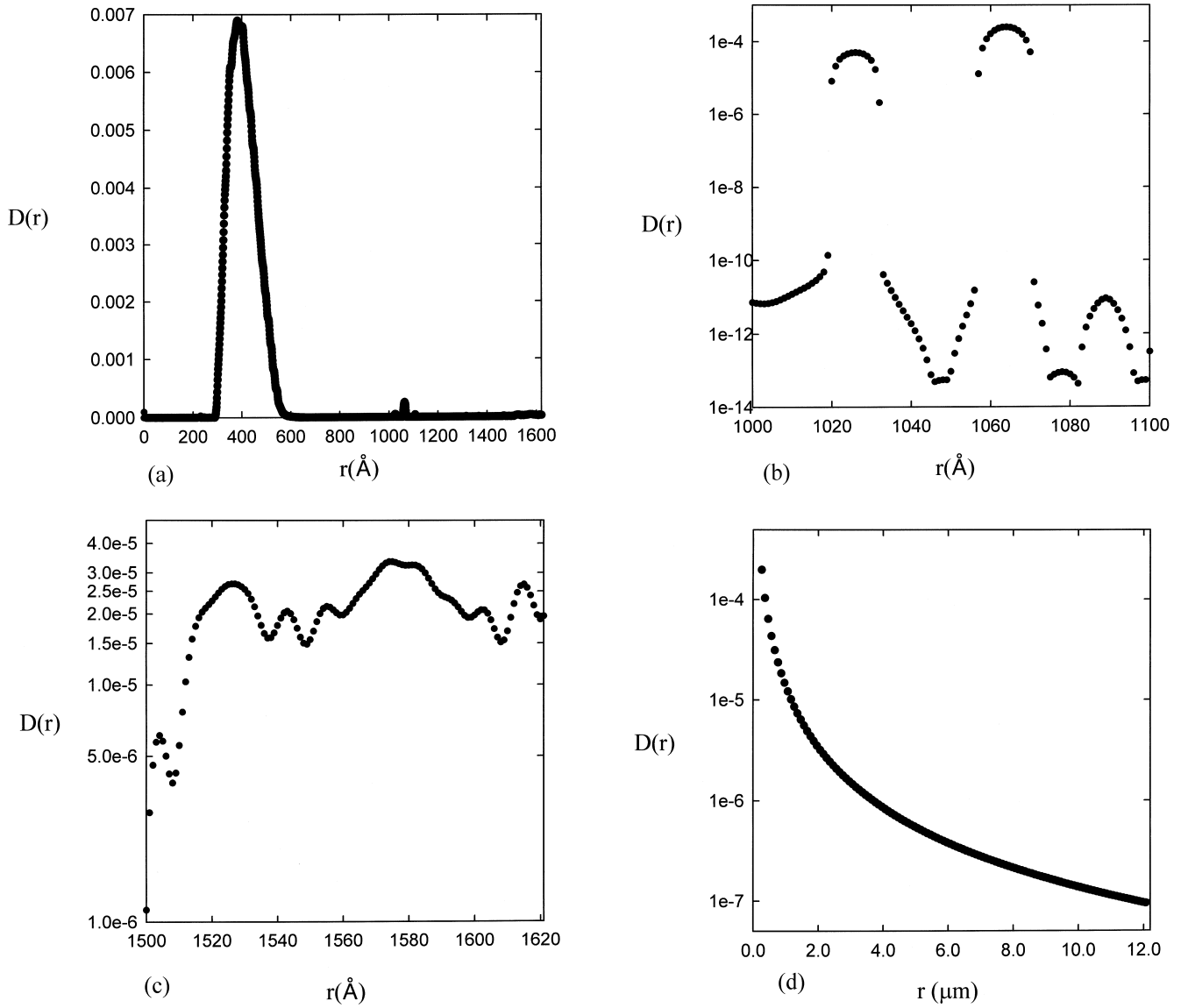

Fig. 2. (a) Distribution function, D(*r*), calculated for SANS data from Mode1 II, modified to include smearing effects (●). (b) Distribution function from Fig. 2a, showing D(*r*) plotted on a log scale in the range $r=1000$–1100 Å (c) distribution function from Fig. 2a, showing D(*r*) plotted on a log scale in the range $r=1500$–1621 Å, (d) distribution function, D(*r*), calculated for USANS data from Mode1 II plotted on a log scale.

show bubbles on the surface ranging in size from $r=1$ to 12.1 μm, with the majority of the bubbles having radii between 1 and 3 μm, and TEM images show a distribution of bubbles between 0.1 and 0.7 μm. This is the approximate form of the distribution calculated from Model II for the USANS data.

Fig. 3a and b compares the calculated intensities from Model II with the experimental data in the q ranges 0–4×10^{-4} Å^{-1} (USANS data) and 0.002–0.32 Å^{-1} (SANS data). Model I is discounted at this point due to the unphysical nature of its distribution function (i.e. many negative values). At this stage it should be mentioned that the experimental data is far from ideal in terms of calculating a distribution function, especially since at large q ($q_{max}=0.32$ Å^{-1}) there is no crossover to a q^{-4} dependence [14]. The USANS experimental data covers a wide size distribution of bubbles from 0.8 to 12.1 μm and the SANS data shows a distribution from 10 Å to several thousand Å. Since there is no crossover to q^{-4} dependence, it is possible that bubbles with radii <10 Å are also present and this is borne out from TEM results [16]. Considering such a wide range of particle sizes and no q^{-4} dependence at high q, it is not surprising that the Model II does not calculate a distribution function which returns a calculated intensity matched exactly to the experimental intensity. However the calculated intensity for the USANS data is close to the experimental intensity for all q, except for $q=0$–0.3×10^{-4} Å^{-1}, and the calculated intensity is close to the experimental intensity for the SANS data from $q=1.94\times10^{-3}$ to 2.4×10^{-2} Å^{-1}, at which point the

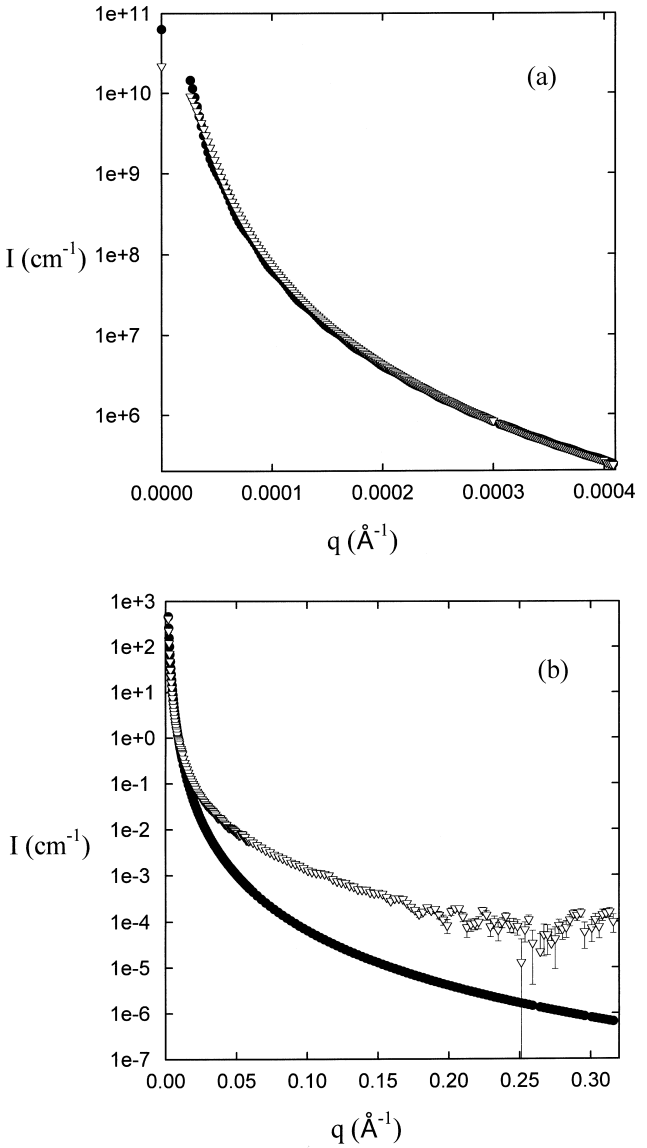

Fig. 3. (a) Comparison of the USANS experimental (q,I) data (▽) with (q,I) calculated from the D(r) determined from Model II (●), plotted on a log scale. (b) Comparison of the SANS experimental (q,I) data (▽) with (q,I) calculated from the D(r) determined from Model II, modified to include smearing effects (●), plotted on a log scale.

agreement between experimental and calculated intensities falls away badly. The lack of agreement between experimental and calculated intensities for the SANS data in the q range 2.4×10^{-2}–0.32 $Å^{-1}$ is most probably due in part to the experimental data lacking a q^{-4} dependence at high q and limitations in the model.

4. Conclusion

The termination corrector method [9,10] (Model I) and the recurrence numerical corrector method [7] (Model II) are used to calculate a distribution function for a difficult data set comprising of SANS and USANS results from the aluminum–hydrogen system. Analysis of the SANS and USANS data combined with INS, TEM and SEM results revealed scattering from a wide size distribution of H_2 bubbles. Model I fails to calculate a physical distribution function, whereas Model II, modified to include smearing effects, calculates a reasonable size distribution, which agrees well with bubble sizes determined from SEM and TEM results [16]. The intensity calculated from the distribution function derived from Model II, agrees reasonably well with the intensity from the USANS data, but there is not good agreement at the high q values of the SANS data.

To the authors knowledge, this is the first attempt to use Model II to calculate a distribution function from experimental data and the results show that by incorporating smearing effects into Model II, it is possible to return a physical distribution function over a wide range of particle sizes. Further efforts should be made to apply the modified version of Model II to small angle scattering data sets. Work is in progress to compare the distribution functions calculated from the modified version of Model II and the maximum entropy method [20] for the preceding SANS and USANS data sets. The calculation of the distribution function of the USANS data, using log normal distribution modeling techniques is also in progress.

Acknowledgements

This research was sponsored in part by the US Department of Energy grant DEFG02-96ER45439. I would also like to thank John Barker and Rick Paul from NIST for the SANS and PGAA experimental results, and Marcelo Mulato from The Universidade Estadual de Campinas, Unicamp, for helpful discussions.

References

[1] G. Kostorz, Materials Science and Technology, Academic Press, New York, 1979.
[2] G. Kostorz, in: H. Brumberger (Ed.), Modern Aspects of Small-Angle Scattering, Kluwer, Dordrecht, Boston, 1995.
[3] A. Guinier, A. Fournet, Small Angle Scattering of X-rays, Wiley, New York, 1955.
[4] P.W. Schmidt, in: H. Brumberger (Ed.), Modern Aspects of Small-Angle Scattering, Kluwer, Dordrecht, Boston, 1995.
[5] M. Agamalian, G.D. Wignall, R. Triolo, Neutron News 9 (1998) 24.
[6] D. Bellmann, M. Klatt, R. Kampmann, R. Wagner, Physica B 241–243 (1998) 71.
[7] M. Mulato, I. Chambouleyron, J. Appl. Cryst. 29 (1996) 29.
[8] D.I. Svergun, A.V. Semenyuk, L.A. Feigin, Acta Crystallogr. A 44 (1988) 244.
[9] O.L. Brill, C.G. Weil, P.W. Schmidt, J. Colloid, Interface Sci. 27 (1968) 479.
[10] O.L. Brill, P.W. Schmidt, J. Appl. Phys. 39 (1968) 2274.
[11] M. Mulato, D. Tygel, I. Chambouleyron, J. Appl. Cryst. 31 (1998) 149.

[12] H.K. Birnbaum, C.E. Buckley, F. Zeides, E. Sirois, P. Rozenak, S. Spooner, J.S. Lin, J. Alloys Compd. 253–254 (1997) 260.
[13] C.E. Buckley, H.K. Birnbaum, Scripta Metall., in preparation.
[14] C.E. Buckley, H.K. Birnbaum, Physica B 241–243 (1998) 344.
[15] I.S. Fedorova, P.W. Schmidt, J. Appl. Cryst. 11 (1978) 405.
[16] C.E. Buckley, H.K. Birnbaum, E. Hollar, D. Bellman, P. Staron, T. Udovic, submitted.
[17] R.M. Lindstrom, J. Res. Nat. Inst. Stand. Tech. 98 (1993) 127.
[18] M. Mulato, D. Tygel, I. Chambouleyron, J. Appl. Cryst. 30 (1997) 808.
[19] J.G. Barker, J.S. Pedersen, J. Appl. Cryst. 28 (1995) 105.
[20] J.A. Potton, G.J. Daniell, B.D. Rainford, J. Appl. Cryst. 21 (1988) 663.